Thermal properties of THz quantum cascade lasers based on different optical waveguide configurations

Miriam S. Vitiello[a] and Gaetano Scamarcio[b]
CNR-INFM Regional Laboratory LIT[3], Dipartimento Interateneo di Fisica "M. Merlin," Università degli Studi di Bari, Via Amendola 173, 70126 Bari, Italy

Vincenzo Spagnolo
CNR-INFM Regional Laboratory LIT[3], Dipartimento Interateneo di Fisica "M. Merlin," Politecnico di Bari, Via Amendola 173, 70126 Bari, Italy

Jesse Alton and Stefano Barbieri[c]
TeraView Limited, 302/304 Science Park, Cambridge CB4 OWG, United Kingdom and Cavendish Laboratory, University of Cambridge, Madingley Road, Cambridge CB3 0HE, United Kingdom

Chris Worrall, Harvey E. Beere, and David A. Ritchie
Cavendish Laboratory, University of Cambridge, Madingley Road, Cambridge CB3 0HE, United Kingdom

Carlo Sirtori
Matériaux et Phénomènes Quantique Laboratory, Université Paris 7, 75251 Paris Cedex 05, France

(Received 5 April 2006; accepted 23 May 2006; published online 13 July 2006)

We compare the thermal properties of THz quantum cascade lasers (QCLs) fabricated with metal-metal optical waveguides based on Au/Au or In/Au wafer bonding. This information was obtained from the analysis of microprobe band-to-band photoluminescence spectra measured on devices operating in continuous wave (cw). The experimental normalized thermal resistances (R_L^*), show that the use of Au/Au wafer bonding optimizes the heat dissipation. Comparison with surface-plasmon based THz QCLs, demonstrates that the use of metal-metal wafer bonding can allow cw operation at progressively higher temperatures. © *2006 American Institute of Physics*.
[DOI: 10.1063/1.2220546]

The recent demonstration of far infrared $GaAs/Al_{0.15}Ga_{0.85}As$ quantum cascade lasers[1] (QCLs) has increased significantly the interest in the THz frequency range, and a variety of components and applications is fueling a rapid progress in this previously underdeveloped spectral region. Increasing the maximum continuous wave (cw) operating temperature of THz QCLs would be highly attractive for a wide range of technological applications. However, one important limit for the thermal performance of THz QCLs is the rather high value of the thermal resistance (15–25 K/W), that is determined by the following factors: (i) the large number of interfaces (1500–2000); (ii) the large active region thickness (>12 μm); (iii) the low thermal conductivity of the $Al_{0.15}Ga_{0.85}As$ alloys; (iv) the thermal coupling between the active region and the heat sink via the waveguide and mounting configurations.

The development of a low-loss waveguide was critical for the realization of THz QCLs due to the dominant free carrier absorption that grows significantly at longer wavelengths. To date, two types of optical waveguides have been implemented, namely, the surface-plasmon (sp),[1,2] and the metal-metal (m-m) waveguides.[3] Both these schemes have also been demonstrated in a buried waveguide geometry.[4]

In this letter we focus on THz QCLs based on m-m waveguides and fabricated with different wafer bonding techniques. Double metal waveguides possess potentially excellent optical properties, due to a mode confinement factor $\Gamma \sim 1$, however, the fabrication of devices with adequate thermal and mechanical properties is strictly related with the wariness during the metal bonding. In particular, we shall show how the careful choice of the metal sequence used for the reactive bonding may lead to a considerable improvement of the device thermal performance. Finally, we compare our results with those obtained on sp based THz QCLs.

In this work we investigated a set of m-m waveguide THz QCLs based on the same active region design, and fabricated with Au/Au (sample *A*) or In/Au (sample *B*) wafer bonding. The conduction and valence band structure of a single period of the active region, calculated at the threshold for lasing are shown in Fig. 1. The quantum design is based on a bound-to-continuum scheme where a miniband is used for the depopulation of the lower laser level via *e*-*e* scattering, while the upper state is designed to fall inside a minigap leading to a diagonal laser transition at υ=2.9 THz.[5]

The 11.57 μm $GaAs/Al_{0.15}Ga_{0.85}As$ thick active region, composed by 90 periods, was grown by molecular beam epitaxy (MBE) between upper (80 nm thick) and lower (700 nm thick) GaAs layers doped to $n=5\times10^{18}$ cm^{-3} and $n=2\times10^{18}$ cm^{-3}, respectively. In both samples only a Ti/Au ($\sim$20 nm/200 nm) layer was deposited on top of the wet etched laser bars. A 1 mm$\times$59 μm double metal device (sample *A*) was bonded to a n^+ GaAs substrate using a 500 nm thick Au bond layer at $\sim$320 °C, while a 0.89 mm $\times$53 μm m-m device (sample *B*) was bonded to the same substrate with a In/Au (1500 nm/500 nm) layer at 250 °C. Devices were then indium bonded to copper holders and mounted on the cold finger of a He flow microcryostat. The cw current-voltage and light-current characteristics measured as a function of the heat sink temperature are plotted in Figs.

[a]Electronic mail: vitiello@fisica.uniba.it
[b]Electronic mail: scamarcio@fisica.uniba.it
[c]Present address: Matériaux et Phénomènes Quantique Laboratory, Université Paris 7, 75251 Paris Cedex 05, France.

0003-6951/2006/89(2)/021111/3/$23.00 © 2006 American Institute of Physics
Downloaded 14 Jul 2006 to 193.204.188.4. Redistribution subject to AIP license or copyright, see http://apl.aip.org/apl/copyright.jsp

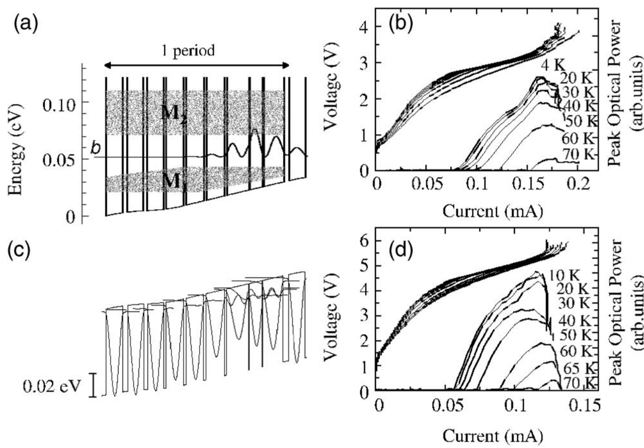

FIG. 1. Conduction (a) and valence (b) band structures of one period of the active region calculated using a self-consistent Schrödinger-Poisson solver at 30 mV per stage, with a 66% conduction band offset. Starting from the injection barrier, the layer sequence of one period, in nanometers is (from right to left): **3.8**/14.0/**0.6**/9.0/**0.6**/15.8/**1.5**/12.8/**1.8**/12.2/**2.0**/12.0/**2.0**/11.4/**2.7**/11.3/**3.5**/11.6. AlGaAs layers are shown in bold, and the underlined GaAs wells are n doped at 1.6 $\times 10^{16}$ cm^{-3}. The shaded area M_1 and M_2 represents the lowest energy and the second minibands, respectively. The wave function square modulus of the excited laser state is labeled as b. (c) and (d) Voltage and emitted power as a function of current measured in cw at different heat sink temperatures, for samples A (c) and B (d).

1(c) and 1(d) for samples A and B. The maximum collected peak power was 300 μW at 4 K for sample A. The photoluminescence spectra were obtained by focusing the 647 nm line of a Kr^+ laser onto the laser facet down to a spot of ≈ 2.5 μm, using an optical power density ~ 200 W/cm^2.[6]

Figures 2(a) and 2(b) show the PL spectra of samples A and B collected under zero pumping current conditions. Each spectrum shows a main band that corresponds to band-to-band transitions between levels in the injector miniband M_1,

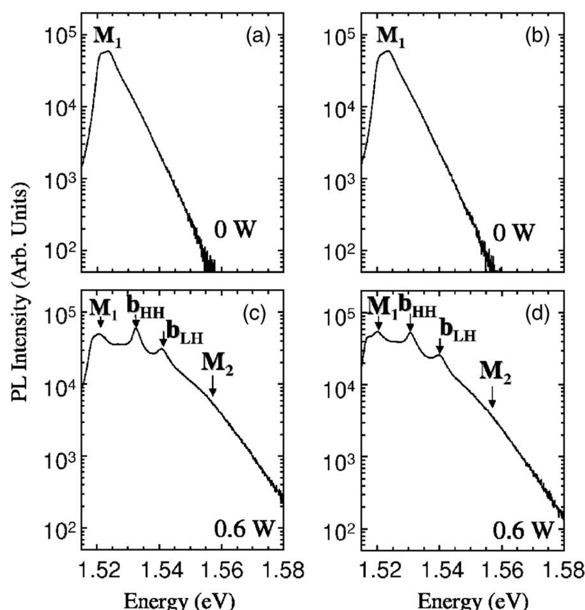

FIG. 2. Representative photoluminescence spectra of samples A [(a) and (c)] and B [(b) and (d)] measured at device off [(a) and (b)] and at P=0.6 W [(c) and (d)], at T_H=45 K. The arrows labeled with M_j mark the energies of the transitions between levels in the conduction minibands (M_j) and valence subbands [see Figs. 1(a) and 1(b)]. The arrows marked with b_{HH} and b_{LH} indicate the heavy-hole and light-hole exciton peaks.

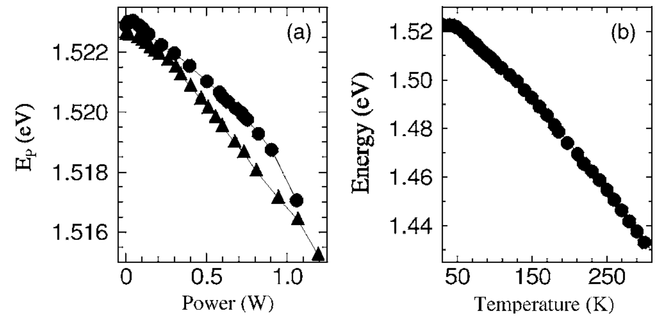

FIG. 3. (a) Peak energy E_P of the PL band labeled with M_1 plotted as a function of P for samples A (●) and B (▼). The lines are guides for the eye. (b) P_L peak energy (E_p) calibration curve of sample A obtained as described in the text. The calibration curve of sample B is identical.

where the vast majority of electrons sits, and valence subbands. In Figs. 2(c) and 2(d) we report the PL spectra collected for samples A and B at an electrical power P=0.6 W. Each spectrum redshifts with P due to the induced Joule heating effect. While the PL band associated with the injector miniband M_1 is still present, additional structures appear on its high energy tail. The two peaks labeled with at b_{HH} and b_{LH} in Figs. 2(c) and 2(d) are ascribed to the heavy-hole (HH) and light-hole (LH) excitons arising from the excited level b when populated by tunnel injection.[7,8] The energy splitting between b_{HH} and b_{LH} is 8.3 (9.3) meV for samples A (B), i.e., $\sim$1.3 ($\sim$2.3) meV higher than what expected in the 14.0–15.8 nm wide GaAs quantum wells,[9] in which level b mainly extends. The measured increase of the HH-LH splitting is expected and ascribed to the residual strain ε_r incorporated at the interfaces as a result of the thermal strain (ε_r) associated with the In/Au and Au/Au wafer bondings. From the measured b_{HH} and b_{LH} PL bands we get the values $\varepsilon_r \sim 8.0 \times 10^{-6}$ and $\varepsilon_r \sim 7.3 \times 10^{-6}$, respectively, for samples A and B.[10] Finally, the broad high energy band labeled with M_2 in Figs. 2(c) and 2(d) is ascribed to transitions involving conduction subbands confined in the active region upper miniband (M_2), progressively populated with the applied electric field.

The redshift of the PL band M_1 of Fig. 2 as a function of P can be used as a thermometric property to extract the device local lattice temperature (T_L). Figure 3(a) shows E_P plotted a function of P for samples A and B. The difference in the measured slopes is ascribed to the stronger electric-field effect calculated for sample B that is $\sim$3 times larger than that measured for sample A. By probing the device at zero-current while varying the heat sink temperature T_H we have determined the PL peak position as a function of T_L, thereby obtaining the calibration curve in the active region of the investigated devices. The calibration curve measured for sample A is plotted in Fig. 3(b). We measured an identical curve for sample B thus demonstrating the excellent reproducibility of the MBE growth. The rather strong temperature dependence of the PL peak energy at temperatures above 80 K ($dE_p/dT \sim 0.25$ meV/K) allows a temperature resolution $\sim$0.5 K. The local temperature of the laser facet was extracted by comparing the shift of the PL peak against the measured calibration curve, taking into account the electric field effect.

The measured T_L values are plotted in Figs. 4(a) and 4(b), respectively, for samples A and B together with the electronic temperatures of the lower ($T_e^{M_1}$) and upper ($T_e^{M_2}$)

Downloaded 14 Jul 2006 to 193.204.188.4. Redistribution subject to AIP license or copyright, see http://apl.aip.org/apl/copyright.jsp

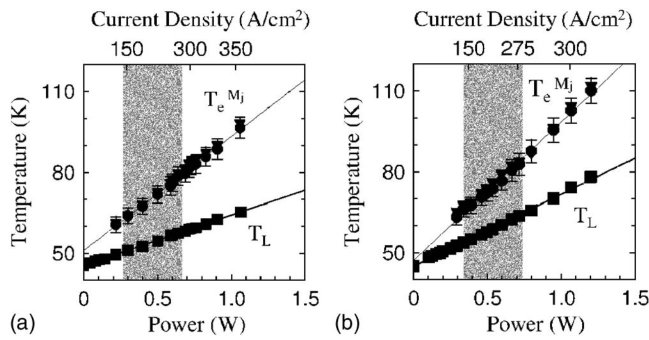

FIG. 4. Mean lattice temperature T_L (■) and miniband electronic temperatures $T_e^{M_1}$ (●), $T_e^{M_2}$ (▼) measured in the active region of the investigated device as a function of P, at T_H=45 K for samples A (a) and B (b). The lines are linear fits to the data. The shaded areas mark the lasing region.

active region minibands. The latter values have been extracted by fitting calculated PL curves to the experimental ones using a similar procedure discussed in Refs. 7 and 11.[12] $T_e^{M_1}$ and $T_e^{M_1}$ are coincident within ~3 K and increase linearly with P with a slope $R_e^{(A)}=42.3$ K/W and $R_e^{(B)}=51.3$ K/W significantly larger than the respective thermal resistances $R_L^{(A)}=dT_L/dP=21.9$ K/W and $R_L^{(B)}=25.5$ K/W. We performed a similar study on a THz QCL based on the same gain medium quantum design of samples *A* and *B* and processed with a sp waveguide[5] (sample *C*) and measured the values $R_L^{(C)}=17.3$ K/W and $R_e^{(C)}=23.2$ K/W.

To compare the thermal properties of the investigated QCLs we have calculated the normalized thermal resistance $R_L^*=R_L\times S/d$, where S and d are the device area and the active region thickness. The results are reported in Table I. The comparison among samples *A*–*C* shows that, in the case of sample *C*, despite the lower thermal resistance mainly due to the significantly larger ridge area typically employed in the fabrication of sp THz QCLs, the R_L^* value is ~4 and 3.4 times larger than that measured for samples *A* and *B*. Our results indicate that although the maximum cw operating temperatures of the investigated bound-to-continuum THz QCLs are identical,[5] the use of m-m waveguides is advantageous to improve the device thermal management. This becomes much more relevant at operating temperatures $T > 100$ K where the Au thermal conductivity is significantly higher than GaAs. Furthermore, the comparison between samples *A* and *B* show that the use of Au/Au interfaces decreases the device R_L^* value leading to a better heat dissipation during cw operation. This can be explained by the higher conductivity of Au with respect to In and also considering that the quality of the In/Au bonding is highly limited from the more difficult adhesion of the metal on the substrate with respect to the Au/Au wafer bonding. In the latter case, we used a Ti layer evaporated prior to the gold acting as a wetting layer and assuring that the gold layer adheres very well to the substrate. These findings are confirmed also by previous experimental reports on THz QCLs.[7,11] We show in Table I the R_L^* values measured on resonant-phonon THz QCLs processed with In/Au (sample *D*) and Cu/Cu (sample *E*) m-m waveguides.[11] In particular, sample *E* shows the lowest value thanks to the higher Cu thermal conductivity. In Table I are also reported the R_L and R_L^* values obtained for a bound-to-continuum THz QCL processed with sp waveguide and based on a different active region scheme[7] (sample *F*) and for a $GaAs/Al_{0.1}Ga_{0.9}As$ THz QCL (sample *G*).[13] The R_L^* value measured for sample *F* is similar to that of sample *C*, thus confirming the advantage to use double metal waveguides to improve the device thermal management. For sample *G* we obtained a R_L^* value ~1.2/1.3 times lower than that of samples *C* and *F*. This reduction can be explained considering that a lower Al mole fraction allows the use of thicker barriers, thus reducing interface roughness scattering and increasing the active region thermal conductivity.[14]

TABLE I. Comparison between the thermal resistances R_L and the parameter $R_L^*=R_L\times S/d$ of a set of investigated THz QCLs, classified on the base of the emission frequency (υ) and waveguide configuration.

Sample	υ (THz)	Waveguide	R_L (K/W)	$R_L^*=R_L\times S/d$ (K×cm/W)
A	2.9	m-mAu/Au	21.9	9.4
B	2.9	m-m In/Au	25.5	11.0
C	2.9	sp	17.3	37.4
D[a]	3.2	m-m In/Au	18.6	12.7
E[a]	2.8	m-mCu/Cu	25.3	7.4
F[b]	2.5	sp	20.1	36.9
G[c]	2	sp	15.6	27.8

[a]Reference 11.
[b]Reference 7.
[c]Reference 13.

CNR-INFM LIT[3] acknowledges financial support from MIUR (DD 1105/2002). The University of Cambridge and Teraview Ltd acknowledge financial support from the E.C. through the IST project Teranova and the PASR 2004 project Terasec. S.B. acknowledges support from the Royal Society.

[1]R. Köhler, A. Tredicucci, F. Beltram, H. E. Beere, E. H. Linfield, A. G. Davies, D. A. Ritche, R. C. Iotti, and F. Rossi, Nature (London) **417**, 156 (2002).
[2]L. Ajili, G. Scalari, D. Hofstetter, M. Beck, J. Faist, H. Beere, G. Davies, E. Linfield, and D. Ritchie, Electron. Lett. **38**, 25 (2002).
[3]B. S. Williams, S. Kumar, H. Callebaut, Q. Hu, and J. L. Reno, Appl. Phys. Lett. **83**, 2124 (2003).
[4]S. S. Dhillon, C. Sirtori, J. Alton, S. Barbieri, H. E. Beere, E. H. Linfield, and D. A. Ritchie, Appl. Phys. Lett. **87**, 071107 (2005).
[5]S. Barbieri, J. Alton, H. E. Beere, J. Fowler, E. H. Linfield, and D. A. Ritchie, Appl. Phys. Lett. **85**, 1674 (2004).
[6]M. S. Vitiello, G. Scamarcio, and V. Spagnolo, Proc. SPIE **6133**, 61330K (2006).
[7]M. S. Vitiello, G. Scamarcio, V. Spagnolo, T. Losco, R. P. Green, A. Tredicucci, H. E. Beere, and D. A. Ritchie, Appl. Phys. Lett. **88**, 241109 (2006).
[8]The Debye screening length is 18–23 nm in the investigated lattice temperature range, while the wave function of level *b* mainly extends in a 59 nm thick spatial region [four right-most quantum wells in Fig. 1(a)] characterized by a negligible static electronic density. This explains the observation of stable excitons associated with level *b* in our samples.
[9]J. Martinez-Pastor, A. Vinattieri, L. Carraresi, M. Colocci, P. Roussignol, and G. Weimann, Phys. Rev. B **47**, 10456 (1993).
[10]Such a difference in the residual strains is expected due to lower thermal expansion coefficient of the Au ($\alpha=14.1\times10^{-6}$ K^{-1}) with respect to that of the In ($\alpha=29.4\times10^{-6}$ K^{-1}).
[11]M. S. Vitiello, G. Scamarcio, V. Spagnolo, B. S. Williams, S. Kumar, Q. Hu, and J. L. Reno, Appl. Phys. Lett. **86**, 111115 (2005).
[12]The fitting procedure was restricted to the range $P\geq0.2$ W ($P\geq0.3$ W), for samples *A* (*B*), where tunnel injection into the upper laser level becomes efficient and the full conduction regime is reached.
[13]C. Worrall, J. Alton, M. Houghton, S. Barbieri, H. E. Beere, D. A. Ritchie, and C. Sirtori, Opt. Express **14**, 171 (2006).
[14]W. S. Capinski, H. J. Maris, T. Ruf, M. Cardona, K. Ploog, and D. S. Katzer, Phys. Rev. B **59**, 8105 (1999).

Downloaded 14 Jul 2006 to 193.204.188.4. Redistribution subject to AIP license or copyright, see http://apl.aip.org/apl/copyright.jsp